Biosensors and Bioelectronics 25 (2010) 2336–2342

Contents lists available at ScienceDirect

Biosensors and Bioelectronics

journal homepage: www.elsevier.com/locate/bios

Biogenic nanoporous silica-based sensor for enhanced electrochemical detection of cardiovascular biomarkers proteins

Kai-Chun Lin[a,1,2], Vindhya Kunduru[b,1,3], Manish Bothara[c,4], Kaushal Rege[a,5], Shalini Prasad[b,*], B.L. Ramakrishna[a,**]

[a] 501 E. Tyler Mall, ECG 303, School of Mechanical, Aerospace, Chemical, and Materials Engineering, Arizona State University, Tempe, AZ 85287-6106, United States
[b] ERC 239, 551 E. Tyler Mall, Department of Electrical Engineering, School of Electrical, Computer and Energy Engineering, Arizona State University, Tempe, AZ 85287, United States
[c] P.O. Box 751, Department of Electrical Engineering, Maseeh College of Engineering, Portland State University, Portland, OR 97207, United States

ARTICLE INFO

Article history:
Received 19 January 2010
Received in revised form 22 March 2010
Accepted 24 March 2010
Available online 2 April 2010

Keywords:
Biogenic silica biosensor
Electrochemical impedance spectroscopy
Protein biomarker detection
Cardiovascular disease

ABSTRACT

The goal of our research is to demonstrate the feasibility of employing biogenic nanoporous silica as a key component in developing a biosensor platform for rapid label-free electrochemical detection of cardiovascular biomarkers from pure and commercial human serum samples with high sensitivity and selectivity. The biosensor platform consists of a silicon chip with an array of gold electrodes forming multiple sensor sites and works on the principle of electrochemical impedance spectroscopy. Each sensor site is overlaid with a biogenic nanoporous silica membrane that forms a high density of nanowells on top of each electrode. When specific protein biomarkers: C-reactive protein (CRP) and myeloperoxidase (MPO) from a test sample bind to antibodies conjugated to the surface of the gold surface at the base of each nanowell, a perturbation of electrical double layer occurs resulting in a change in the impedance. The performance of the biogenic silica membrane biosensor was tested in comparison with nanoporous alumina membrane-based biosensor and plain metallic thin film biosensor. Significant enhancement in the sensitivity and selectivity was achieved with the biogenic silica biosensor, in comparison to the other two, for detecting the two protein biomarkers from both pure and commercial human serum samples. The sensitivity of the biogenic silica biosensor is ~1 pg/ml and the linear dose response is observed over a large dynamic range from 1 pg/ml to 1 μg/ml. Based on its performance metrics, the biogenic silica biosensor has excellent potential for development as a point of care handheld electronic biosensor device for detection of protein biomarkers from clinical samples.

1. Introduction

Proteomics research has resulted in the identification of a number of biomarker proteins, which have the potential to greatly improve disease diagnosis (Darain et al., 2004; Hahm and Lieber, 2004; Nam et al., 2003; Niwa et al., 1990). Detection of multiple biomarkers has been identified as a diagnostic mechanism to provide the information necessary for robust diagnosis of a disease in any person within a population (Abeloff et al., 2000; Chou et al., 2004; Danesh et al., 1998). Widespread use of protein biomarkers in healthcare will ultimately depend upon the development of techniques that allow rapid and multiplexed detection of a wide range of biomarkers with high selectivity and sensitivity.

The enzyme linked immunosorbent assay (ELISA), a fluorescent optical detection method, is the "gold standard" for clinical diagnostics with sensitivity down to about 3 picogram/ml (pg/ml) (Biocompare-Manual, 2008). Electrical detection of protein biomarkers is a relatively new approach that monitors a specific electrical parameter that undergoes change during the protein detection event. The advent of nanotechnology in the field of clinical diagnostics has resulted in the incorporation of nanoscale materials in designing diagnostics assays, especially for electrical detection. The major classes of nanomaterials that have been used for protein biomarker detection are: nanotubes, nanowires, nanoparticles and nanotemplates (Rusling et al., 2009; Suni, 2008). Often these materials have been utilized for their improved surface area towards developing detectors with enhanced sensitivity and reduced use of reagents. The use of carbon nanotubes for cancer protein biomarker detection and cancer therapy has been demonstrated (Kam et al., 2005). Implementation of the field effect transistor based transconductance technique using silicon

* Corresponding author. Tel.: +1 480 727 9670; fax: +1 480 965 8118.
** Corresponding author. Tel.: +1 480 965 6560; fax: +1 480 965 1500.
E-mail addresses: shalini.prasad.1@asu.edu, sprasad5@asu.edu (S. Prasad), BRamakrishna@asu.edu (B.L. Ramakrishna).
[1] These authors contributed equally to this work.
[2] Tel.: +1 480 727 9314; fax: +1 480 965 1500.
[3] Tel.: +1 480 965 8218; fax: +1 480 965 8218.
[4] Tel.: +1 503 725 3814; fax: +1 503 725 4224.
[5] Tel.: +1 480 727 8616; fax: +1 480 727 3292.

0956-5663/$ – see front matter © 2010 Elsevier B.V. All rights reserved.
doi:10.1016/j.bios.2010.03.032

nanowires has made it possible to detect proteins with sensitivity in the range of picogram/ml–femtogram/ml (Zheng et al., 2005). The use of antibody-coated nanoparticles as electrical biosensors operating on electrochemical conductance technique has resulted in sensitivities in the range of lower nanogram/ml (ng/ml) to a few hundred pg/ml (Willner et al., 2003). The use of silicon nanoporous templates for protein detection has been demonstrated with sensitivity in pg/ml (Bothara et al., 2008). In all the nanomaterial based electrical protein biosensors, detection response is on the order of minutes with very low sample volume, typically on the order of nanoliters.

While, each of these nanomaterial-enabled proteomic biosensors have demonstrated impressive performance metrics, there is a paucity of rigorous studies to benchmark these new technologies against the standard clinical diagnostics assay-ELISA, where detection occurs in a multiwell microtiter plate. Among the four nanomaterial classes mentioned above, nanotemplates can be most easily configured to generate a proteomic assay similar in geometrical configuration to the ELISA assay and this has led to the design of nanotemplate based electrical biosensor assays. We expect that by generating such an assay we will be able to benchmark the biosensor performance with respect to ELISA, enabling a quicker penetration into the domain of portable diagnostics assays.

In our prior work, we have proposed a biosensor assay architecture utilizing nanoporous alumina membranes that mimics the multi well architecture of an ELISA plate (Bothara et al., 2008). A nanoporous alumina membrane is overlaid onto the base microelectrode generating a high-density array of nanoscale voids, also known as nanowells, on a single metallic sensing site. Each nanowell functions in a similar manner as that of a well in ELISA plates with the detected proteins bound to the base of the well. There are three key differences between the nanomonitor nanowells and the micro wells of ELISA. First, protein detection is achieved by measuring the perturbation to the electrical double layer in the nanowells resulting in an electrochemical impedance change, whereas in the micro wells quantification of fluorescence is a measure of the protein-binding event. Second, the measured electrical signal due to the electrical double layer perturbation is cumulative of the signals generated from an array of nanowells on a single microscale sensing site, where as in the case of micro wells each well is interrogated and quantified individually. Third, protein binding and detection is achieved through measuring single interactions between the primary antibody and the protein (antigen) in the nanowells, where as in the micro well proteomic assay there are two capture steps associated with the protein detection. The first step being the capture of the protein by the immobilized primary antibody and the second capture step the binding of the secondary antibody tagged with the flurophore to the primary antibody-antigen complex. These differences lead to (a) improved antigen-antibody association by increasing the antibody capture density within the nanowells, (b) enhanced detected signal strength due to signal accumulation from arrays of nanowells and (c) reduced the assay time due to protein detection through single capture step.

Nanoporous alumina membrane has been employed for the detection of penicillin up to 0.1 ng/ml through electrochemical conductance measurement (Takhistov, 2004). We used nanoporous alumina in our earlier work (Bothara et al., 2008) for building the electrical immunoassay-based biosensor due to the following reasons: (a) elimination of the capacitance leakage between individual nanopores because alumina is a good electrical insulator (b) reduced interference from electrical noise due to the thermal shielding and (c) biocompatibility of the material in electrical biosensing. Despite these advantages, the manufactured nanoporous alumina membranes have a number of limitations, which can significantly impact the biosensor performance. They are (a) absence of simple chemistries to achieve surface functionalization of the side walls of the nanopores in the nanoporous alumina membrane making it difficult to leverage the side walls of the membrane to improve the detection sensitivity and (b) absence of simple chemistries to adhere the alumina onto the sensing site which is essential to minimize background noise signals.

In the current work we have designed and fabricated a biosensor using biogenic silica from diatoms as the nanoporous template, which we have heterogeneously integrated on to the microelectrode platform. Though alumina and silica surfaces appear to be somewhat similar, there are significant differences, namely, (a) Si–O is much more covalent than the Al-O bond (50% covalent character in silica vs. 35% in alumina), and therefore, substitution reactions are more facile in silica (b) alumina surface is not as stable at pH below 8 and there are surface charges caused by lattice defects (Popat et al., 2004) (c) surface hydroxyl groups of hydrated alumina are less acidic than those on silica surface because, the isoelectric point of alumina, which is an indication of the ionization of the surface hydroxyl groups $Al–OH \rightarrow AlO^- + H^+$, is attained at pH 9, while that for silica is reached at pH 2 (Benesi and Winquist, 1978).

Diatoms offer an alternative approach to engineering nanoscale systems because of the ability to design materials that are inspired by or adapted from biologically produced nanostructures. Diatoms are eukaryotic, unicellular photosynthetic algae that are well known for the spectacular design of their silica-based cell walls (Round et al., 1990), and ubiquitous presence in nearly every aquatic habitat on earth. Diatoms produce diverse three-dimensional, regular silica structures (aka frustules) with pores from nanometer to micrometer dimensions. These biogenic silica nanostructures derived from diatoms possess several unique properties (Parkinson and Gordon, 1999) including, (1) A porous hierarchical nanostructure that enhances diffusion of species through the highly ramified network of micro and nanopores which facilitates “molecular traffic control”. (2) The ability to undergo a variety of surface modifications through well-established chemistries that allow with ease the tethering of biomolecules (Townley et al., 2008). (3) Flexibility of design through the availability of a variety of shapes, sizes, and symmetries, from more than a hundred of thousand species of diatoms. (4) The potential for confinement enhancements in sensitivity because of the nanoscale pore structure. The enormous surface area (>200 m^2/g for fresh diatom shells) also makes them a promising platform for sensors in general and biosensors, in particular. (5) Finally, these silica-based templates also offer the advantage of easier integration with conventional well-established processing methods in the semiconductor industry.

The potential of diatoms as biosensors has been demonstrated previously. For example, photoluminescence generated by the biogenic silica frustules of diatoms has been employed as the physical transducing effect to detect the biomolecular interaction of complementary DNA chains (De Stefano et al., 2009), and antibody–antigens (Gale et al., 2009). However, all of the studies so far have employed optical detection schemes.

We believe that the present work is the first reported study of using diatoms as part of a sensor configuration that employs changes in electrical properties to selectively and quantitatively detect antibody–antigen interactions. We have demonstrated the performance of this multi scale assay as a biosensor by detecting two inflammatory proteins; C-reactive protein (CRP) and myeloperoxidase (MPO). These two inflammatory proteins have been selected from a review of the literature for acute coronary syndrome (ACS) and are histologic participants that constitute a vulnerable plaque. In recent years the research focus has been on identifying the presence of the two protein markers CRP and MPO on the patho-physiology of vulnerable coronary plaque rupture (Baldus et al., 2003; Mach et al., 1997). Hence in this paper we have focused our efforts on (a) detecting two specific pro-

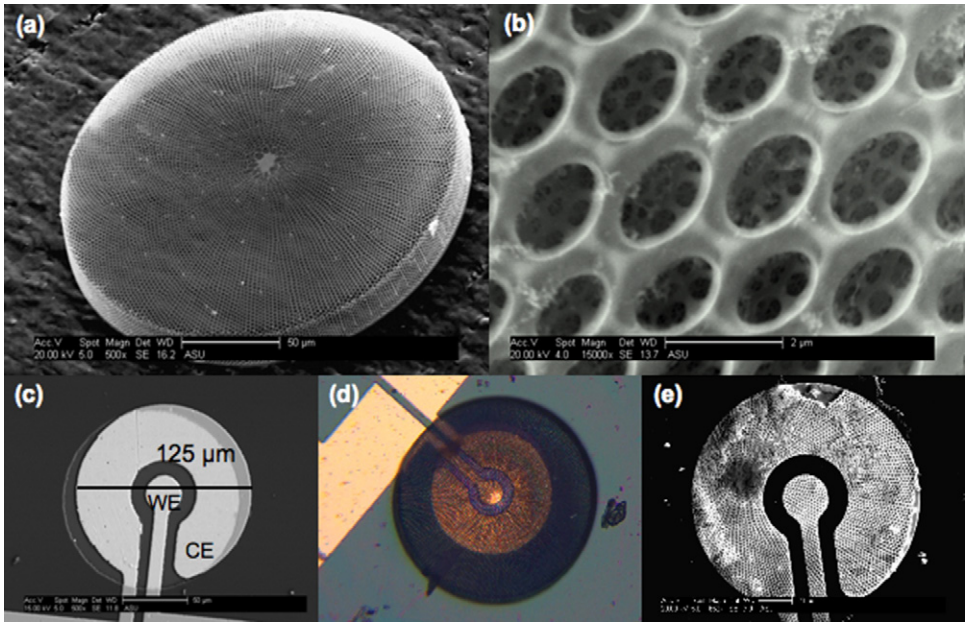

Fig. 1. SEM and optical images of electrode and *Coscinodiscus* frustules on the chip: (a) *Coscinodiscus* frustule imaged by SEM, outer surface facing up; (b) Inner surface consisting of the vertical chambers; (c) SEM image of gold electrode on the chip; (d) Optical image and (e) SEM image of a *Coscinodiscus* frustule on the gold electrode.

teins – CRP and MPO in isotonic buffer as well as in human serum (b) enhancing the detection performance i.e. improving the sensitivity and reducing the cross-reactivity more specifically from human serum samples such that the detection performance comparable to ELISA. We show that the use of diatoms significantly enhances the sensitivity as compared to nanoporous alumina membranes.

2. Materials and methods

2.1. Configuration of the diatom-based biosensor

The diatom species *Coscinodiscus wailesii* was chosen because of its rather large diameter (100–200 μm) that can completely cover the gold electrodes (Fig. 1a) and because of its hierarchical pore structure and good symmetry (Losic et al., 2006). The siliceous cell wall has a honeycomb structure consisting of the vertical chambers arranged in hexagonal symmetry with porous plates forming the floor and the roof of the honeycomb (Fig. 1b). In this particular diatom species, the outer surface (floor) of the plate, which in touch with external environment (Fig. 2a), is perforated by highly symmetric nanoscale pores, where as the internal surface (roof) of the plate, which is in contact with the algal cell, exhibits a single microscale pore in the center of each honeycomb. It was purchased from the Provasoli-Guillard National Center for Culture of Marine Phytoplankton (CCMP) at the Bigelow Marine Laboratory. Cells were cultured in f/2 seawater medium at 20 °C under continuous photoperiod. The diatoms were cleaned by the addition of 50% (v/v) hydrogen peroxide (30% solution) and incubation at 90 °C for 1–2 h to remove organic materials. Samples were centrifuged at 3000 rpm for 5 min, and washed with nanopure water for several times, and stored in 70% ethanol solution. These treatments cause the diatom frustule to be separated into two frustule valves and a girdle band.

The microelectrode chips comprising of metallic gold sensing sites were first coated with polylysine by treatment with 0.01% aqueous solution of polylysine. In order to place a diatom frustule on the electrode, one drop of cleaned diatom frustule suspension was deposited on the polylysine-coated chips (Fig. 1c and d). Micromanipulation and attachment of an individual diatom frustule onto the electrode was performed using KRN-09 Positioner (J MicroTechnology, USA). The diatom frustule was positioned such that the outer surface (floor) of the porous plate, which has the nanoscale pores, is in contact with the metallic gold sensing site, which forms

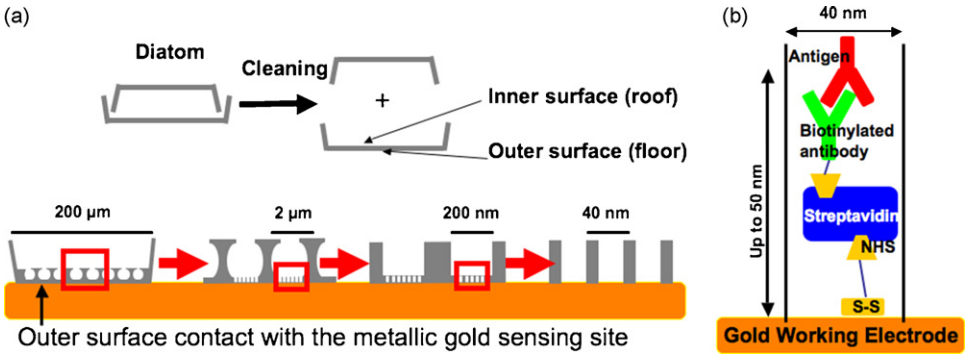

Fig. 2. (a) Schematic model of frustule pore architecture for the diatom placed on the gold working electrode, (b) schematic showing the antibody–antigen binding inside a nanowell, (c) equivalent circuit of a sensing site.

the base of the nanowell of the biosensor (Fig. 2a). SEM images were acquired using a Philips XL-30 field-emission scanning electron microscope operated at 15–20 kV to visually verify that the positioned diatom frustules completely covered an individual metallic gold sensing site (Fig. 1e). Hence each sensing site comprised of a working and a counter electrode. The diameter of the working electrode (WE) was 25 μm and the diameter of the counter electrode (CE) was five times larger. Electrical measurements were obtained across the WE and CE.

2.2. Electrical impedance spectroscopy (EIS)

The protein binding and detection process is achieved by incorporating an immunoassay into each nanowell of the biosensor. All the biomolecules (linker molecules, antibodies and antigens) have surface charges. The binding of these molecules to the base of each nanowell perturbs the charge distribution in the electrical double layer that forms at the solid/liquid interface (Bothara et al., 2008; Reddy et al., 2008). This charge perturbation produces a capacitance change in the electrical double layer (Fig. 2b) (Bothara et al., 2008; Yang et al., 2007). The biomolecule binding induced capacitance change can be measured by the electrical impedance spectroscopy technique. This technique is widely used in electrical biosensors for detecting surface charged analytes (Bothara et al., 2008; Darain et al., 2004; Desilva et al., 1995; Takhistov, 2004). In this technique a low AC voltage is provided as the input to a sensing site, which functions as the electrical stimulus to direct the surface charged biomolecules onto a sensing site. The binding of the biomolecules produces a change in the measured output impedance across a sensing site (Bothara et al., 2008; Yang et al., 2007). The measured impedance is the sum total of two components, the resistance and capacitance of the sensing site. It is only the capacitive component that is a measure of the biomolecule binding event, as the capacitive component indicates the surface charge differential in the electrical double layer as a function of biomolecule binding (Bothara et al., 2008; Katz and Willner, 2003; Pei et al., 2001). Hence the input voltage parameters (frequency and voltage amplitude) need to be optimized to measure this capacitive component.

We determined that an AC voltage of 100 mV at a frequency of 1 kHz when applied between the WE and CE of a sensing site enabled the measurement of the changes to the capacitive component associated with the protein-binding event. When the biomolecules are added to the biosensor device, they cause the electrical double layer (EDL) to move upwards resulting in a change in capacitance. Hence monitoring the capacitance change in the EDL is a measure of the protein-binding event. An increase in antigen concentration will in turn increase the capacitance change in the EDL. The EDL is approximately 20–50 nm in height, hence capacitance changes primarily due to biomolecule binding that occurs in this region. The equivalent electrical circuit of a sensing site is modeled after a Randell's electrochemical cell and comprises of a resistor and two capacitors. The resistor is a measure of the bulk resistance of the buffer solution, R_{sol}, due to the ions present in the bulk regions of the nanowells (>50 nm from base of the nanowell). The dielectric capacitance between the two electrodes, due to the base substrate is represented by C_{de}. This capacitance does not change for varying input AC voltage frequencies and hence this capacitance is accounted for when the biosensor is calibrated during baseline/control measurements. The electrical double layer capacitance is represented by C_{dl}, which undergoes a change due to the biomolecule based perturbation to the EDL (Gamry 600-Potentiostat, Gamry Instruments, Warminster, PA). The measured C_{dl} capacitance is a sum of the contributions from the WE and CE nanowells. Based on electrochemistry, it has been determined that the bulk resistive component dominates the impedance measurements at high frequencies (>10 kHz) and the capacitive double layer component dominates the impedance measurements at low frequencies (1 kHz and lower) (Gomez et al., 2001; Lasseter et al., 2004; Pei et al., 2001). We experimentally identified 1 kHz to be the optimum frequency for operating the biosensor after evaluating the biosensor performance over a frequency range from 50 Hz to 10 kHz. At 100 mV and 1 kHz we observed maximum change in the EDL capacitance with minimum background electrical noise.

2.3. Biosensor surface treatment

The antigens CRP, MPO and the biotinylated monoclonal antibodies for these two proteins were all purchased from Calbiochem, San Diego, CA. The monoclonal antibodies were used for the detection assay in order to increase specificity. The gold surface at the base of the nanowells was functionalized with dithiobis (succinimidyl propionate) (DSP, Pierce Chemicals, St. Louis, MO). DSP (Fig. 2b), a covalent linker, has a thiol (sulfur) end group that has great affinity to gold (Balamurugan et al., 2008; Riepl et al., 1999). Hence the thiol end of the linker binds to the gold base of the nanowell and the NHS end group at the opposite epitope of the linker is available to bind to streptavidin. The entire gold base surface of the nanowell was saturated with DSP linker molecules prior to injecting streptavidin. 10 μl of streptavidin at a dose of 100 μg/ml was injected into the diatom nanowells. After 30 min room temperature incubation, the nanowells were washed three times with 0.15 M PBS. The dose concentration of streptavidin was identified empirically to ensure saturation of the nanowell surfaces. 10 μl of the biotinylated antibody was then injected onto the nanowells and after a 15 min incubation at room temperature was washed thrice with 0.15 M PBS. The saturation doses of the two antibodies were determined experimentally as detailed in the results section. The antibody-saturated surface was then treated with 10 μl of 100 μg/ml of Bovine Serum Albumin (BSA, Pierce Chemicals, St. Louis, MO) to ensure blocking of any unbound surfaces of the nanowells. After 15 min incubation at room temperature the nanowells were washed thrice with 0.15 M PBS. 10 μl of 0.15 M PBS was then injected onto the sensing site and AC input voltage (100 mV, 50 Hz–1 kHz) was applied across working electrode (WE) and counter electrode (CE) of each sensing site. The impedance from each sensing site was obtained, which corresponded to the zero dose measurements. After aspirating the 0.15 M PBS solution, 10 μl of the lowest dose of the antigen was added to the sensing site of the biosensor surface, after 15-min incubation at room temperature the impedance was measured using EIS. Typically steady state measurements were obtained within 15 min of injection of the test antigen sample. After the measurement of the impedance the sensing site was washed thrice with 0.15 M PBS. Fig. 2b is the schematic representation of the binding of the biomolecules for detection of the proteins within the nanopores of the diatom. The same process was repeated for the next highest dose of the antigen for the entire range of doses of the antigen. For the detection of the antigens from human serum, after saturating the diatom nanowells with the antibody, 10 μl of commercial human serum free of CRP and MPO was injected into the diatom nanowells. After steady state was achieved, the impedance value was noted as the baseline. Aliquots of both the antigens were prepared in the antigen free commercial human serum (GIBCO, Invitrogen, San Diego, CA) for the range of doses. The dose response was performed in a manner similar to that of the dose response for antigens when aliquoted in 0.15 M PBS. Changes in impedance were measured for the various doses of the two proteins and the change was expressed as a percentage change with respect to the PBS baseline for the pure samples and as a percentage change with respect to human serum base line for the serum-spiked samples. The impedance changes associated with each dose of the antigen were expressed as percentage change with respect to the impedance measured from PBS/antigen free human serum interac-

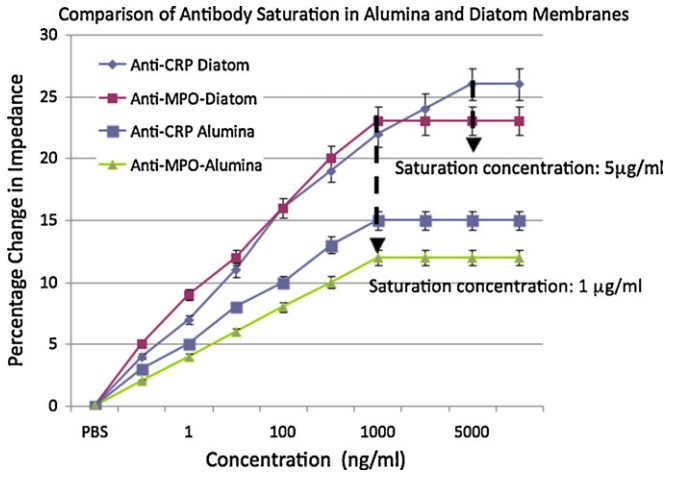

Fig. 3. Saturation isotherm for the two antibodies on the alumina and diatom substrates, respectively. The percentage change in impedance from the baseline associated with antibody saturation is higher on the diatom (26%, anti-CRP and 23% anti-MPO) as compared to alumina (15%, anti-CRP and 12% anti-MPO). The saturation dose for anti-CRP was 5 μg/ml and 1 μg/ml on the diatom and alumina surfaces, respectively, whereas the saturation dose of anti-MPO was 1 μg/ml on both the alumina and diatom substrates.

tion on the antibody-saturated sensor surface for each specific dose of the antigen.

3. Results and discussion

This section shows the results from initial control experiments, dose response attained for two proteins CRP and MPO in pure buffer and human serum samples from (i) planar gold microelectrodes, (ii) alumina membranes overlaid on to the gold microelectrodes and (iii) diatom membranes overlaid onto the gold microelectrodes. The discussion of the results is included in the sections under the headings (a) antibody saturation isotherms, (b) protein dose response from pure buffer and serum samples and (c) selectivity analysis.

3.1. Antibody saturation isotherm

The first set of experiments was performed to identify the dose of the antibody that would saturate the sensor surface. The impedances have been shown at the detection frequency of 1 kHz, as noted in the experimental section. (All measurements were taken from three different sensing sites. The measurements from the three different sites were averaged and the average error margin for the data is shown per dose.) Starting from a lower concentration (1 ng/ml) of the monoclonal antibodies, nanomembrane-overlaid sensor platform was treated in a stepwise manner with increasing concentration of the antibodies. At 5 μg/ml for anti-CRP and 1 μg/ml for anti-MPO, impedance reached saturation with the diatom membrane and the saturation doses for alumina were 1 μg/ml for anti-CRP as well as for anti-MPO as shown in Fig. 3. There was 26%, 15% and 6% change from baseline for anti-CRP saturation from diatom, alumina membranes and planar gold respectively and 22%, 12% and 9% change from baseline for anti-MPO saturation from diatom, alumina membranes and planar gold respectively. This corresponds to a 1.5–2 times increase in the relative signal as we go from alumina to diatom-based sensors, and 1.5–2.5 times increase is seen from gold to alumina. The percentage change in impedance from the baseline was considerably higher on the diatom membrane as compared to the alumina membrane, and higher for the alumina membrane than that for just the gold film.

It is tempting to assign the increase in the measured signal strength to the increase in surface area on going from planar gold to alumina to diatom. But, the surface area of the 200 nm pores in the alumina membrane that is exposed to the gold electrode is estimated to be 25%, where as, the surface area of the 40 nm pores in the diatom membrane that is exposed to the gold electrode is only 5% (data in Supplementary section). Therefore, the observed increase cannot be explained purely on the basis of surface areas. However, when one calculates the pore densities (40 pores of 40 nm diameter per 1 μm^2) it is seen that the pore density in the diatom is five times larger than in the alumina membrane. Hence, the results obtained from antibody saturation indicate that the enhanced confinement offered by the diatom nanopores is perhaps playing a decisive role. Confinement-induced enhancement of antibody–antigen interactions has been postulated earlier (Krishnamoorthy and Himmelhaus, 2008) to explain the increase of sensitivity due to nanopatterning the surface of a sensor. It has been shown to be particularly effective when the surface is tailored within a few multiples of the antibody–antigen size (Krishnamoorthy and Himmelhaus, 2008). We believe that the pore structure of the diatom that has been used in the present experiment (Fig. 2b) offers a topography that is conducive for a confinement-induced enhancement. Further work is being carried out to control the size and chemistry of the smallest pore structure and to test different combinations of molecular couples in order to assess the generality of our explanation.

In our previous studies on nanoporous alumina (Bothara et al., 2008), we have observed increased sensitivity compared to the native gold film. This obviously cannot be explained by increased surface area and we have suggested that spatial confinement of the protein biomolecules within the nanopores in could be playing a role. This phenomenon may be physically correlated to macromolecular crowding of proteins in cellular systems that enable protein efficacy and functionality. Within cellular systems, the cytoplasm inside of the cell is typically “crowded” with a complex dispersion of proteins and ions. Unlike the intra cellular environment, protein detection in in-vitro environments such as the biosensor platforms is performed in relatively less dense or “crowded” environments, which are thought to significantly affect the protein efficacy and hence adversely influence the detection of these proteins. To attain the crowding effects within biosensor platforms, the packing density of the protein biomolecules is significantly increased through biomolecule confinement in the nanoporous platforms, which is believed to contribute to enhancing the sensitivity of detection.

3.2. Protein dose response from pure and serum samples

We performed the dose response for the two proteins CRP and MPO over a concentration range from 1 pg/ml to 1 μg/ml.). It was observed that the percentage change in impedance increased with the increase in concentration of the antigens over this concentration range. Saturation of the impedance values was not observed over this concentration range. The percentage changes in the impedance were significantly higher during the antigen dose response on diatom membrane as compared to the alumina membrane and planar gold electrodes. The percentage change in impedance from PBS baseline ranged from 60% (MPO), 58% (CRP) on diatom, 38% (MPO) 30% (CRP) on alumina and 22% (MPO), 20% (CRP) on planar gold for the two proteins when aliquoted in PBS over the protein dose range of 1 pg/ml to 1 μg/ml as shown in Fig. 4a. The percentage change in impedance from human serum baseline ranged up to 42% (MPO), 40% (CRP) on diatom, 33% (MPO), 26% (CRP) on alumina and 15%(MPO) 12% (CRP), on planar gold electrodes for the two proteins when aliquoted in human serum as shown in Fig. 4b.

The limit of detection was found to be 1 pg/ml for CRP and MPO in pure samples on diatom membranes and 100 pg/ml on alumina

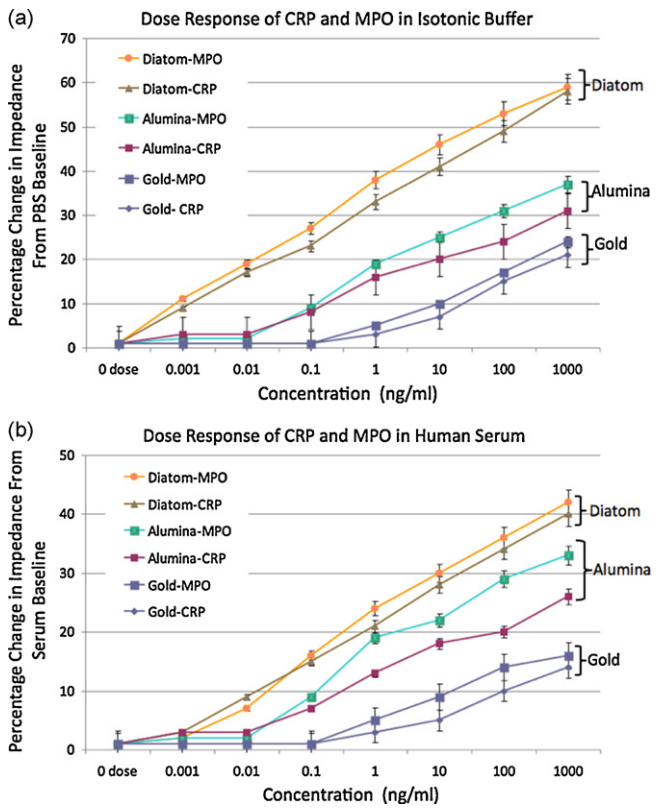

Fig. 4. Dose response of the two proteins CRP and MPO. (a) The proteins were aliquoted in isotonic buffer samples and were evaluated over a detection regime from 1 pg/ml to 1 μg/ml. The maximum changes in the impedance from base line for the two proteins were obtained from the diatom substrates as compared o the alumina and gold substrates. (b) Protein dose response for proteins aliquoted in commercial human serum. Similar to the isotonic buffer samples, maximum changes to the impedance were observed from the diatom substrate as compared to the alumina and gold substrates. The changes in impedance for a comparable dose were much lower from the serum samples as compared to the isotonic buffer samples for a specific substrate.

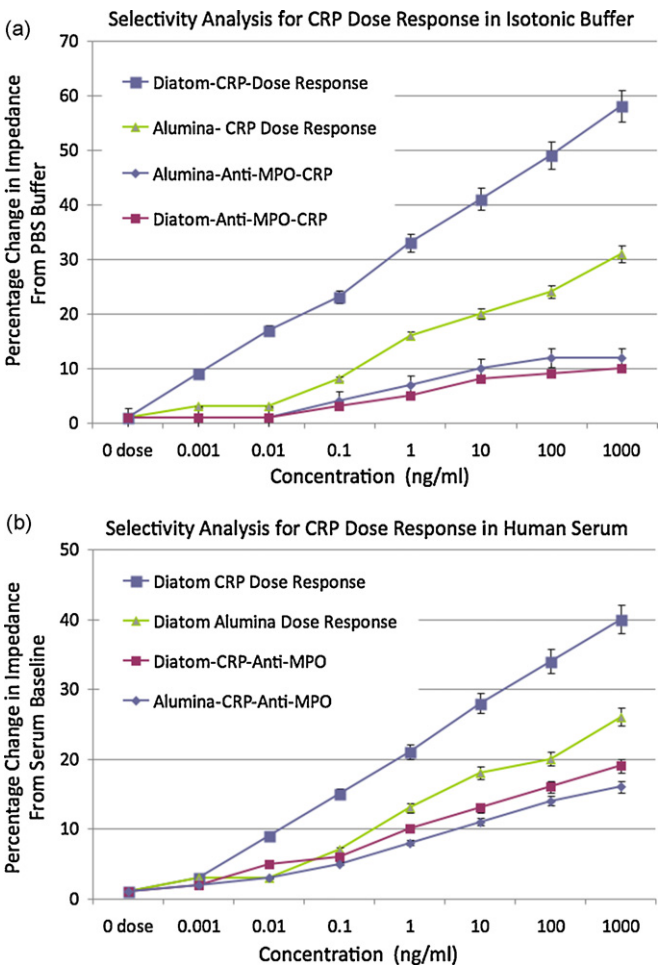

Fig. 5. Demonstration of selectivity in detection of the protein CRP in isotonic buffer and in human serum samples (a) dose response of CRP aliquoted in isotonic buffer on anti-CRP and anti-MPO saturated diatom and alumina substrates. (b) Dose response of CRP aliquoted in human serum on anti-CRP and anti-MPO saturated diatom and alumina substrates.

membranes and 1 ng/ml on planar gold electrodes as shown in Fig. 4a. Similarly the limit of detection was 10 pg/ml on diatom membranes, 500 pg/ml on alumina membranes and 5 ng/ml for planar gold electrodes for CRP and MPO detection from human serum samples. For proteins in pure buffer, 10-fold increase is seen in sensitivity upon use of nanoporous alumina membrane as compared to gold and a 100-fold increase is realized on going from alumina to diatom. In serum a 10-fold increase is seen from gold to alumina and a 50-fold increase is seen on going from alumina to diatom.

3.3. Selectivity analysis

A key feature in identifying the potential of the diatom biosensor towards clinical applicability is to identify its performance in robustly and specifically detecting a targeted antigen from complex samples. In order to simulate these conditions we have identified and compared the percentage changes to the impedance of the diatom biosensor in detecting the two proteins markers CRP and MPO aliquoted in PBS and commercial human serum over the dose range from 1 pg/ml to 1 μg/ml, on their respective antibody-saturated diatom surfaces as well as on the non-specific antibody-saturated surfaces (CRP on anti-MPO surface and MPO on anti-CRP surface). These sets of experiments were performed to identify the cross-reactivity of the pure and serum protein samples on similar inflammatory protein receptors. An impedance change of 58% and 30% from base line was observed for CRP dose response on anti-CRP saturated diatom and alumina substrates with the protein samples aliquoted in isotonic buffer samples. Comparatively 10% and 11% change in impedance was observed for CRP aliquoted in isotonic buffer on anti-MPO saturated diatom and alumina substrates respectively (Fig. 5a). In the case of CRP proteins samples aliquoted in human serum, 40% and 26% from base line was observed for CRP dose response on anti-CRP saturated diatom and alumina substrates respectively. Comparatively 19% and 16% change in impedance was observed for CRP aliquoted in human serum on anti-MPO saturated diatom and alumina substrates respectively (Fig. 5b).

In the case of MPO aliquoted in isotonic buffer, 60% and 38% change in impedance was observed over the dose range of 1 pg/ml to 1 μg/ml on anti-MPO saturated diatom and alumina substrates, respectively. Comparatively a 10% change in impedance for MPO samples was observed over the same dose range on anti-CRP saturated substrates. For MPO samples aliquoted in human serum impedance changes of 42% and 33% from base line was observed for MPO dose response on anti-MPO saturated diatom and alumina substrates respectively. Comparatively 22% and 17% change in impedance was observed for MPO on anti-CRP saturated diatom and alumina substrates respectively (data in Supplementary section). Therefore these is a nearly two-fold increase in impedance for any given dose in the dose response for both the proteins on the specific antibody-coated substrate as compare to the non-specific antibody-saturated substrate either in PBS

or in human serum samples. Confinement of the biomolecules into the nanoporous sensor platform have been thought to be attributed with the enhanced sensitivity and selectivity observed from the porous surfaces. High cross-reactivity in the alumina membrane as compared to the diatom membrane may be attributed to increase in non-specific adsorption of antigens onto the sensor surface due to the absence of a hierarchical porous structure. Higher sensitivity and selectivity in isotonic buffer that in commercial serum is because buffer samples are purer as far as proteins are concerned. The commercial human serum has more possibilities for interference and cross-reactivity.

4. Conclusions

The design of the diatom membrane-based biosensor is believed to significantly contribute to the enhanced detection strength translating to enhanced sensitivity of the biosensor. Approximately three times enhancement in the impedance changes from planar gold surfaces and twice the improvement in impedance changes as compared to manufactured alumina nanopore surfaces have been demonstrated for individual doses over the dose response range. The diatom membrane surface enables robust detection of the two inflammatory markers in commercial human serum samples at the lower picogram/ml dose regime, which is a clinically significant dose regime in identifying patient risk to cardiovascular disease. The five characteristics viz. response time, dynamic range, signal strength, sensitivity and selectivity, which are critical for a successful sensor, are all enhanced for the diatom-based sensor. The faster response time and the enhanced sensitivity may be attributed to the enhanced diffusion of fluids in nano channels (Daiguji et al., 2004), which in this case would be the nanowells. The linear dynamic range of detection extended from 1 pg/ml to 1 μg/ml (six orders of magnitude), which is much higher than ELISA (1–2 orders) (Keshishian et al., 2009). The diatom-based sensor exhibits an increase by nearly a factor of two in the relative signal as compared to alumina-based sensors. For proteins in pure buffer, 10-fold increase is seen in sensitivity upon use of nanoporous alumina membrane as compared to gold and a 100-fold increase is realized on going from alumina to diatom. In serum a 10-fold increase is seen from gold to alumina and a 50-fold increase is seen on going from alumina to diatom. Specificity studies have revealed that there is a two-fold increase in impedance for any given dose in the dose response for both the proteins on the specific antibody-coated substrate as compared to the non-specific antibody-saturated substrate either in PBS or in human serum samples. In context of detecting the protein biomarkers for vulnerable coronary plaque rupture: CRP and MPO the detection sensitivity of the diatom biosensor is in the pg/ml regime both in isotonic buffer as well as human serum samples which is well below the clinically relevant concentration regime of the ng/ml to the lower mg/ml essential to predict a patient's risk for the disease.

In summary, the diatom biosensor could be used as a rapid, label-free screen for selectively detecting disease biomarkers and can be developed as a lateral flow immunoassay device due to the rapid and significantly enhanced impedance changes to the measured electrical impedance due to the binding of the protein biomolecules. There is enormous potential of operating this device is in "real-life" conditions to distinguish between low and high cardiovascular risk by detecting proteins in clinically relevant concentrations.

Appendix A. Supplementary data

Supplementary data associated with this article can be found, in the online version, at doi:10.1016/j.bios.2010.03.032.

References

Abeloff, M.D., Armitage, J.O., Lichter, A.S., Niederbuber, J.E., 2000. Clinical Oncology, 2nd ed. Churchill Livingstone, New York.

Balamurugan, S., Obubuafo, A., Soper, S.A., Spivak, D.A., 2008. Anal. Bioanal. Chem. 390 (4), 1009–1021.

Baldus, S., Heeschen, C., Meinertz, T., Zeiher, A.M., Eiserich, J.P., Munzel, T., Simoons, M.L., Hamm, C.W., Investigators, C., 2003. Circulation 108 (12), 1440–1445.

Benesi, H.A., Winquist, B.H.C., 1978. Surface Acidity of Solid Catalysts. Advances in Catalysis. Academic Press, pp. 97–182.

Biocompare-Manual, C-Reactive Protein ELISA Kits From Helica Biosystems, Inc., http://www.biocompare.com/review/1106/C-Reactive-Protein-ELISA-Kits-From-Helica-Biosystems-Inc.html.

Bothara, M., Venkatraman, V., Reddy, R.K.K., Barrett, T., Carruthers, J., Prasad, S., 2008. Nanomedicine (UK) 3 (4), 423–436.

Chou, S.F., Hsu, W.L., Hwang, J.M., Chen, C.Y., 2004. Biosens. Bioelectron. 19 (9), 999–1005.

Daiguji, H., Yang, P., Szeri, A.J., Majumdar, A., 2004. Nano Lett. 4 (12), 2315–2321.

Danesh, J., Collins, R., Appleby, P., Peto, R., 1998. J. Am. Med. Assoc. 279 (18), 1477–1482.

Darain, F., Park, D.S., Park, J.S., Shim, Y.B., 2004. Biosens. Bioelectron. 19 (10), 1245–1252.

De Stefano, L., Rotiroti, L., De Stefano, M., Lamberti, A., Lettieri, S., Setaro, A., Maddalena, P., 2009. Biosens. Bioelectron. 24 (6), 1580–1584.

Desilva, M.S., Zhang, Y., Hesketh, P.J., Maclay, G.J., Gendel, S.M., Stetter, J.R., 1995. Biosens. Bioelectron. 10 (8), 675–682.

Gale, D.K., Gutu, T., Jiao, J., Chang, C.H., Rorrer, G.L., 2009. Adv. Funct. Mater. 19 (6), 926–933.

Gomez, R., Bashir, R., Sarikaya, A., Ladisch, M.R., Sturgis, J., Robinson, J.P., Geng, T., Bhunia, A.K., Apple, H.L., Wereley, S., 2001. Biomed. Microdev. 3, 201–209.

Hahm, J., Lieber, C.M., 2004. Nano Lett. 4 (1), 51–54.

Kam, N., O'Connell, M., Wisdom, J.A., Dai, H., 2005. Proc Natl Acad Sci USA 102 (33), 11600–11605.

Katz, E., Willner, I., 2003. Electroanalysis 15 (11), 913–947.

Keshishian, H., Addona, T., Burgess, M., Mani, D.R., Shi, X., Kuhn, E., Sabatine, M.S., Gerszten, R.E., Carr, S.A., 2009. Mol. Cell. Proteomics 8 (10), 2339–2349.

Krishnamoorthy, S., Himmelhaus, M., 2008. Adv. Mater. 20 (14), 2782–2788.

Lasseter, T.L., Cai, W., Hamers, R.J., 2004. Analyst 129 (1), 3–8.

Losic, D., Rosengarten, G., Mitchell, J.G., Voelcker, N.H., 2006. J. Nanosci. Nanotechnol. 6 (4), 982–989.

Mach, F., Lovis, C., Gaspoz, J.M., Unger, P.F., Bouillie, M., Urban, P., Rutishauser, W., 1997. Eur. Heart. J., 1897–1902.

Nam, J.M., Thaxton, C.S., Mirkin, C.A., 2003. Science 301 (5641), 1884–1886.

Niwa, O., Morita, M., Tabei, H., 1990. Anal. Chem. 62 (5), 447–452.

Parkinson, J., Gordon, R., 1999. Trends Biotechnol. 17 (5), 190–196.

Pei, R.J., Cheng, Z.L., Wang, E.K., Yang, X.R., 2001. Biosens. Bioelectron. 16 (6), 355–361.

Popat, K.C., Mor, G., Grimes, C.A., Desai, T.A., 2004. Langmuir 20 (19), 8035–8041.

Reddy, R.K., Bothara, M.G., Barrett, T.W., Carruthers, J., Prasad, S., 2008. IEEE Sens. J. 8 (5–6), 720–723.

Riepl, M., Mirsky, V.M., Novotny, I., Tvarozek, V., Rehacek, V., Wolfbeis, O.S., 1999. Anal. Chim. Acta 392 (1), 77–84.

Round, F., Crawford, R., Mann, D., 1990. The Diatoms: Biology and Morphology of the Genera. Cambridge University Press, Cambridge, UK.

Rusling, J.F., Sotzing, G., Papadimitrakopoulosa, F., 2009. Bioelectrochemistry 76 (1–2), 189–194.

Suni, I.I., 2008. Trend. Anal. Chem. 27 (7), 604–611.

Takhistov, P., 2004. Biosens. Bioelectron. 19 (11), 1445–1456.

Townley, H.E., Parker, A.R., White-Cooper, H., 2008. Adv. Funct. Mater. 18 (2), 369–374.

Willner, I., Shipway, A.N., Willner, B., 2003. ACS Symp. Ser. 844, 88–105.

Yang, W.S., Butler, J.E., Russell, J.N., Hamers, R.J., 2007. Analyst 132 (4), 296–306.

Zheng, G.F., Patolsky, F., Lieber, C.M., 2005. Abstr. Pap. Am. Chem. Soc. 229, U782.